SCIENCE CHINA
Physics, Mechanics & Astronomy

• Research Paper •

July 2010 Vol.53 No.7: 1325–1332
doi: 10.1007/s11433-010-4013-2

A nonlinear POD reduced order model for limit cycle oscillation prediction

CHEN Gang*, LI YueMing & YAN GuiRong

MOE Key Laboratory for Strength & Vibration, College of Aerospace, Xi'an Jiaotong University, Xi'an 710049, China

Received November 24, 2009; accepted March 15, 2010; published online June 9, 2010

As the amplitude of the unsteady flow oscillation is large or large changes occur in the mean background flow such as limit cycle oscillation, the traditional proper orthogonal decomposition reduced order model based on linearized time or frequency domain small disturbance solvers can not capture the main nonlinear features. A new nonlinear reduced order model based on the dynamically nonlinear flow equation was investigated. The nonlinear second order snapshot equation in the time domain for proper orthogonal decomposition basis construction was obtained from the Taylor series expansion of the flow solver. The NLR 7301 airfoil configuration and Goland+ wing/store aeroelastic model were used to validate the capability and efficiency of the new nonlinear reduced order model. The simulation results indicate that the proposed new reduced order model can capture the limit cycle oscillation of aeroelastic system very well, while the traditional proper orthogonal decomposition reduced order model will lose effectiveness.

reduced-order model, limit cycle oscillation, proper orthogonal decomposition, aeroelasticity

PACS: 47.11.-J, 47.52.+j, 47.40.-x, 47.40.Hg

With the development of computational aeroelasticity, the aeroelastic response can be accurately predicted by the high-fidelity physics-based mathematical model such as computational fluid dynamics (CFD) and computational structure dynamics (CSD) couple solver. However, the computation cost is too large for these high-fidelity methods to be applied to the multidisciplinary conception design with many iterations. Unlike high-fidelity couple solver, the reduced order model (ROM) aims to construct a simple mathematical representation model, which can capture the dominating behavior of aeroelastic system and can be conveniently used in conception design, control and data-driven systems [1].

Many approaches for constructing linear flow based aeroelastic ROMs have been developed and were shown to produce numerical results which compare well with high-fidelity nonlinear solver. Among these approaches, the reduced order model based on proper orthogonal decomposition (POD/ROM)has become the most popular method. For example, the POD/ROM was successfully applied to the CFD-based aeroelastic analysis of airfoil [2], wing [3] and full aircraft [4], especially in flutter prediction [3–5]. Most of the currently proposed ROMs are typically constructed based on the linearized time or frequency domain small disturbance solvers, which are dynamically linearized about the nonlinear steady mean background flow.

Most aeroelastic phenomena such as flutter and gust response can be dealt with these ROMs based on dynamically linearization methods. But unfortunately, some important strong nonlinear dynamics with large structure deformation can not be simulated by the small disturbance solvers, for example, limit cycle oscillation (LCO) [6,7]. There are seldom successful reports about the traditional time-domain POD/ROM to predict LCO generated by nonlinear aerodynamics. Although the first order frequency-domain har-

*Corresponding author (email: aachengang@mail.xjtu.edu.cn)

monic balance POD (HB/POD) solver developed by Dowell et al. [8] can capture LCO very well in some instances, there are still obvious errors in other instances far away from the frequency where the ROM was created.

Modeling the cases where the amplitude of the unsteady flow oscillation is large or large changes occur in the mean background flow requires the ROMs for dynamically nonlinear solvers, because the linearized time or frequency domain small disturbance solvers can not capture the main nonlinear features [6,7]. Such ROMs are essential for matched point flutter onset analysis as well as nonlinear LCO analysis. We will develop a new dynamically nonlinear solver based POD/ROM, or called NPOD/ROM, which will enable the rapid modeling of nonlinear unsteady aerodynamic flows and the associated fluid forces, especially for the LCO prediction. NPOD/ROM intends to extend the conventional dynamically linear POD snapshot equation to dynamically nonlinear snapshot equation by second order Taylor serials expansion in the time domain .This means that the traditional POD/ROM is the first order model, while the NPOD/ROM is the second order model. The NLR 7301 Airfoil Configuration and Goland+ wing/store aeroelastic system are used to validate the capability and efficiency of the new nonlinear NPOD/ROM.

1 The POD algorithm

For one series data $\{x^k\}$, $x^k \in \mathbb{C}^n$ of n-dimension space, which is called snapshot in POD method, search a m-dimension proper orthogonal subspace $\boldsymbol{\Psi} \in \boldsymbol{R}^{n\times m}$ to minimize the mapping errors from $\{x^k\}$ to $\boldsymbol{\Psi}$:

$$G = \min_{\Phi} \sum_{k=1}^{m} \left\| x^k - \boldsymbol{\Phi}\boldsymbol{\Phi}^H x^k \right\| = \sum_{k=1}^{m} \left\| x^k - \boldsymbol{\Psi}\boldsymbol{\Psi}^H x^k \right\|, \boldsymbol{\Phi}^H\boldsymbol{\Phi} = \boldsymbol{I}, \quad (1)$$

It is equal to

$$\boldsymbol{H} = \max_{\Phi} \sum_{k=1}^{m} \frac{\left\langle \left(x^k, \boldsymbol{\Phi}\right)^2 \right\rangle}{\left\|\boldsymbol{\Phi}\right\|^2} = \sum_{k=1}^{m} \frac{\left\langle \left(x^k, \boldsymbol{\Psi}\right)^2 \right\rangle}{\left\|\boldsymbol{\Psi}\right\|^2}, \quad \boldsymbol{\Phi}^H\boldsymbol{\Phi} = \boldsymbol{I}, \quad (2)$$

$(\cdot,\cdot)$ is an inner product, and $\langle\cdot\rangle$ is the mean value operator. If the snapshot matrix is computed by a numerical simulation, the $\langle\cdot\rangle$ can be neglected. The constraint optimization problem of eq. (2) can be transformed into Lagarange equation:

$$J\left(\boldsymbol{\Phi}\right) = \sum_{k=1}^{m} \left(x^k, \boldsymbol{\Phi}\right)^2 - \lambda\left(\left\|\boldsymbol{\Phi}\right\| - 1\right). \quad (3)$$

Solve the partial derivative objective function $J(\boldsymbol{\Phi})$ to $\boldsymbol{\Phi}$, and we could get

$$\frac{\mathrm{d}}{\mathrm{d}\boldsymbol{\Phi}} J\left(\boldsymbol{\Phi}\right) = 2\boldsymbol{X}\boldsymbol{X}^H\boldsymbol{\Phi} - 2\lambda\boldsymbol{\Phi}, \quad (4)$$

$\boldsymbol{X} = \left\{x^1 \quad x^2 \quad \cdots \quad x^m\right\}$ is the snapshot matrix, consisting of snapshots. Let eq. (4) equal zero. There is

$$\left(\boldsymbol{X}\boldsymbol{X}^H - \lambda\boldsymbol{I}\right)\boldsymbol{\Psi} = 0, \quad (5)$$

eq. (5) is a real symmetry eigenvalue problem of POD kernel $\boldsymbol{K}=\boldsymbol{X}\boldsymbol{X}^H$. For high order $\boldsymbol{K} \in \boldsymbol{R}^{n\times n}$, the large eigenvalue problem is not easy to solve. Considering $\boldsymbol{X}\boldsymbol{X}^H$ and $\boldsymbol{X}^H\boldsymbol{X}$ have the same eigenvalue, we can obtain $\boldsymbol{\Psi}$ from the follow lower m-dimension problem:

$$\begin{cases} \boldsymbol{X}^H\boldsymbol{X}\boldsymbol{V} = \boldsymbol{V}\boldsymbol{\Lambda}, \\ \boldsymbol{\Psi} = \boldsymbol{X}\boldsymbol{V}\boldsymbol{\Lambda}^{-1/2}, \end{cases} \quad (6)$$

$\boldsymbol{\Psi} = \left[\psi_1 \quad \psi_2 \quad \cdots \quad \psi_m\right]$, $\boldsymbol{\Lambda} = \mathrm{diag}\left(\lambda_1 \quad \lambda_2 \quad \cdots \quad \lambda_m\right)$, $\lambda_1 \geqslant \lambda_2 \geqslant \cdots \geqslant \lambda_m$. Truncate Ψ to r-order vector $\boldsymbol{\Psi}_r = \left[\psi_1 \quad \psi_2 \quad \cdots \quad \psi_r\right]$, the full system $x^{n\times 1}$ can be reduced to a r-order system:

$$x^{n\times 1} = \boldsymbol{\Psi}_r \xi^{r\times 1}. \quad (7)$$

2 NPOD/ROM method

2.1 Aeroelastic equation

The full-coupled nonlinear aeroelastic equation decentralized by finite volume method for flow and finite element method for structure is:

$$\frac{\mathrm{d}\boldsymbol{A}\left(\boldsymbol{u},\dot{\boldsymbol{u}}\right)\boldsymbol{w}}{\mathrm{d}t} + \boldsymbol{R}\left(\boldsymbol{w},\boldsymbol{u},\dot{\boldsymbol{u}}\right) = 0, \quad (8)$$

$$M v_{,t} + f^{\mathrm{int}}\left(u,v\right) = f^{\mathrm{ext}}\left(u,w\right). \quad (9)$$

For the flow equation, $\boldsymbol{w}$ is the conservative flow field value including flow velocity, flow density and enthalpy. $\boldsymbol{R}$ is flux value, $\boldsymbol{A}$ is the fluid cell volume, $\boldsymbol{u}$ is structure general displacement, and $\boldsymbol{v}$ is structure general displacement derivatives. For structure equation, $\boldsymbol{M}$ is mass matrix, $\boldsymbol{f}^{\mathrm{int}}$ is structure inner force and $\boldsymbol{f}^{\mathrm{ext}}$ is the aerodynamic loads acting on the structure.

2.2 Dynamically nonlinear flow equation

2.2.1 Nonlinear snapshot equation

In order to reduce the flow system, first, compute the value of the operator $(\cdot,\cdot)$ and $\langle\cdot\rangle$, or the covariant matrix of the unsteady flow parameters, which are the so-called snapshots. For the FVM-decentralized NS equation, at the convergent steady flow ($\boldsymbol{w}_0$, $\boldsymbol{u}_0$, $\dot{\boldsymbol{u}}_0$) as a given reference flow condition, we have

$$\frac{\mathrm{d}\boldsymbol{A}(\boldsymbol{u}_0,\dot{\boldsymbol{u}}_0)\boldsymbol{w}_0}{\mathrm{d}t}=\boldsymbol{R}(\boldsymbol{w}_0,\boldsymbol{u}_0,\dot{\boldsymbol{u}}_0)=0,$$

$$\boldsymbol{R}(\boldsymbol{w},\boldsymbol{u},\dot{\boldsymbol{u}})=0,\dot{\boldsymbol{w}}_0=0,\boldsymbol{u}_0=0,\dot{\boldsymbol{u}}_0=0,\ddot{\boldsymbol{u}}_0=0.$$

Suppose $(\delta\boldsymbol{w},\delta\boldsymbol{u},\delta\dot{\boldsymbol{u}})$ is the flow perturbation around the nonlinear steady solver $(\boldsymbol{w}_0,\boldsymbol{u}_0,\dot{\boldsymbol{u}}_0)$ and then expand the flow eq. (8) at $(\boldsymbol{w}_0,\boldsymbol{u}_0,\dot{\boldsymbol{u}}_0)$ by the Taylor serials. The first item of eq. (8) is

$$\begin{aligned}&\boldsymbol{A}(\boldsymbol{u},\dot{\boldsymbol{u}})\dot{\boldsymbol{w}}+\left(\boldsymbol{w}\frac{\partial A}{\partial\boldsymbol{u}}\right)\cdot\dot{\boldsymbol{u}}+\left(\boldsymbol{w}\frac{\partial A}{\partial\dot{\boldsymbol{u}}}\right)\cdot\ddot{\boldsymbol{u}}\\&=\boldsymbol{A}(\boldsymbol{u},\dot{\boldsymbol{u}})\dot{\boldsymbol{w}}+\boldsymbol{E}\cdot\dot{\boldsymbol{u}}+\boldsymbol{D}\cdot\ddot{\boldsymbol{u}}.\end{aligned}\tag{10}$$

Considering that the accuracy of the geometry conservation law of FVM method is second order, the third order effect or the gird acceleration effect can be ignored and the last item of eq. (10) is also ignored. Retaining the second order items of Taylor serials of the above equation, we obtain

$$\begin{aligned}\boldsymbol{A}(\boldsymbol{u},\dot{\boldsymbol{u}})\dot{\boldsymbol{w}}&=A(\boldsymbol{u}_0+\delta\boldsymbol{u},\dot{\boldsymbol{u}}_0+\delta\dot{\boldsymbol{u}})(\dot{\boldsymbol{w}}_0+\delta\dot{\boldsymbol{w}})\\&=\boldsymbol{A}(\boldsymbol{u}_0+\delta\boldsymbol{u},\dot{\boldsymbol{u}}_0+\delta\dot{\boldsymbol{u}})\delta\dot{\boldsymbol{w}}\\&=\left[\boldsymbol{A}(\boldsymbol{u}_0,\boldsymbol{o})+\left(\frac{\partial A}{\partial\boldsymbol{u}}\right)_0\delta\boldsymbol{u}+\left(\frac{\partial A}{\partial\dot{\boldsymbol{u}}}\right)_0\delta\dot{\boldsymbol{u}}\right]\delta\dot{\boldsymbol{w}},\end{aligned}\tag{11}$$

$$\begin{aligned}\boldsymbol{E}\dot{\boldsymbol{u}}&=\boldsymbol{E}_0\cdot\dot{\boldsymbol{u}}_0+\boldsymbol{E}_0\cdot\delta\dot{\boldsymbol{u}}+\left(\frac{\partial\boldsymbol{E}}{\partial\boldsymbol{w}}\delta\boldsymbol{w}+\frac{\partial\boldsymbol{E}}{\partial\boldsymbol{u}}\delta\boldsymbol{u}+\frac{\partial\boldsymbol{E}}{\partial\dot{\boldsymbol{u}}}\delta\dot{\boldsymbol{u}}\right)_0\cdot\dot{\boldsymbol{u}}_0\\&\quad+\left(\frac{\partial\boldsymbol{E}}{\partial\boldsymbol{w}}\delta\boldsymbol{w}+\frac{\partial\boldsymbol{E}}{\partial\boldsymbol{u}}\delta\boldsymbol{u}+\frac{\partial\boldsymbol{E}}{\partial\dot{\boldsymbol{u}}}\delta\dot{\boldsymbol{u}}\right)_0\delta\dot{\boldsymbol{u}}\\&=\boldsymbol{E}_0\cdot\delta\dot{\boldsymbol{u}}+\left(\frac{\partial A}{\partial\boldsymbol{u}}\delta\boldsymbol{w}+\boldsymbol{w}\frac{\partial^2\boldsymbol{A}}{\partial\boldsymbol{u}^2}\delta^2\boldsymbol{u}+\boldsymbol{w}\frac{\partial^2\boldsymbol{A}}{\partial\boldsymbol{u}\partial\dot{\boldsymbol{u}}}\delta\dot{\boldsymbol{u}}\delta\boldsymbol{u}\right)_0\delta\dot{\boldsymbol{u}}\\&=\boldsymbol{w}_0\frac{\partial A}{\partial\boldsymbol{u}}(\boldsymbol{u}_0)\cdot\delta\dot{\boldsymbol{u}}+\left(\frac{\partial A}{\partial\boldsymbol{u}}\right)_0\delta\boldsymbol{w}\delta\dot{\boldsymbol{u}}.\end{aligned}\tag{12}$$

By expanding the second item of the equation and neglecting the third order item, there is

$$\begin{aligned}\boldsymbol{R}(\boldsymbol{w},\boldsymbol{u},\dot{\boldsymbol{u}})&=\boldsymbol{R}(\boldsymbol{w}_0,\boldsymbol{u}_0,\dot{\boldsymbol{u}}_0)+\left(\frac{\partial\boldsymbol{R}}{\partial\boldsymbol{w}}\right)_0\delta\boldsymbol{w}+\left(\frac{\partial\boldsymbol{R}}{\partial\boldsymbol{u}}\right)_0\delta\boldsymbol{u}\\&\quad+\left(\frac{\partial\boldsymbol{R}}{\partial\dot{\boldsymbol{u}}}\right)_0\delta\dot{\boldsymbol{u}}+\frac{1}{2!}\left(\frac{\partial}{\partial\boldsymbol{w}}\delta\boldsymbol{w}+\frac{\partial}{\partial\boldsymbol{u}}\delta\boldsymbol{u}+\frac{\partial}{\partial\dot{\boldsymbol{u}}}\delta\dot{\boldsymbol{u}}\right)_0^2\\&\quad\times\boldsymbol{R}(\boldsymbol{w},\boldsymbol{u},\dot{\boldsymbol{u}})\\&=\frac{1}{2}\left(\frac{\partial^2\boldsymbol{R}}{\partial^2\boldsymbol{w}}\right)_0\delta^2\boldsymbol{w}\\&\quad+\left[\left(\frac{\partial\boldsymbol{R}}{\partial\boldsymbol{w}}\right)_0+\left(\frac{\partial^2\boldsymbol{R}}{\partial\boldsymbol{w}\partial\boldsymbol{u}}\right)_0\delta\boldsymbol{u}+\left(\frac{\partial^2\boldsymbol{R}}{\partial\boldsymbol{w}\partial\dot{\boldsymbol{u}}}\right)_0\delta\dot{\boldsymbol{u}}\right]\delta\boldsymbol{w}\\&\quad+\frac{1}{2}\left(\frac{\partial^2\boldsymbol{R}}{\partial^2\boldsymbol{u}}\right)_0\delta^2\boldsymbol{u}+\frac{1}{2}\left(\frac{\partial^2\boldsymbol{R}}{\partial^2\boldsymbol{w}}\right)_0\delta^2\dot{\boldsymbol{u}}\\&\quad+\left(\frac{\partial^2\boldsymbol{R}}{\partial\boldsymbol{u}\partial\dot{\boldsymbol{u}}}\right)_0\delta\boldsymbol{u}\delta\dot{\boldsymbol{u}}+\left(\frac{\partial\boldsymbol{R}}{\partial\boldsymbol{u}}\right)_0\delta\boldsymbol{u}+\left(\frac{\partial\boldsymbol{R}}{\partial\dot{\boldsymbol{u}}}\right)_0\delta\dot{\boldsymbol{u}}.\end{aligned}\tag{13}$$

The total second order Taylor serials or the discrete NS equation can be rearranged by $\delta\boldsymbol{w}$:

$$\begin{aligned}&\left[A(\boldsymbol{u}_0,\boldsymbol{o})+\left(\frac{\partial A}{\partial\boldsymbol{u}}\right)_0\delta\boldsymbol{u}+\left(\frac{\partial A}{\partial\dot{\boldsymbol{u}}}\right)_0\delta\dot{\boldsymbol{u}}\right]\delta\dot{\boldsymbol{w}}+\frac{1}{2}\left(\frac{\partial^2\boldsymbol{R}}{\partial^2\boldsymbol{w}}\right)_0\delta^2\boldsymbol{w}\\&+\left[\left(\frac{\partial\boldsymbol{R}}{\partial\boldsymbol{w}}\right)_0+\left(\frac{\partial A}{\partial\boldsymbol{u}}\right)_0\delta\dot{\boldsymbol{u}}+\left(\frac{\partial^2\boldsymbol{R}}{\partial\boldsymbol{w}\partial\boldsymbol{u}}\right)_0\delta\boldsymbol{u}+\left(\frac{\partial^2\boldsymbol{R}}{\partial\boldsymbol{w}\partial\dot{\boldsymbol{u}}}\right)_0\delta\dot{\boldsymbol{u}}\right]\delta\boldsymbol{w}\\&+\frac{1}{2}\left(\frac{\partial^2\boldsymbol{R}}{\partial^2\boldsymbol{u}}\right)_0\delta^2\boldsymbol{u}+\frac{1}{2}\left(\frac{\partial^2\boldsymbol{R}}{\partial^2\dot{\boldsymbol{u}}}\right)_0\delta^2\dot{\boldsymbol{u}}+\left(\frac{\partial^2\boldsymbol{R}}{\partial\boldsymbol{u}\partial\dot{\boldsymbol{u}}}\right)_0\delta\boldsymbol{u}\delta\dot{\boldsymbol{u}}\\&+\left(\frac{\partial\boldsymbol{R}}{\partial\boldsymbol{u}}\right)_0\delta\boldsymbol{u}+\left[\boldsymbol{w}_0\frac{\partial A}{\partial\boldsymbol{u}}(\boldsymbol{u}_0)+\left(\frac{\partial\boldsymbol{R}}{\partial\dot{\boldsymbol{u}}}\right)_0\right]\delta\dot{\boldsymbol{u}}=0.\end{aligned}\tag{14}$$

The accuracy of the spatial decentralization scheme is no more than the third order, and the derivatives of flux to grid displacement and velocity are much bigger than the second order partial derivatives. The non-dimensional $\delta\boldsymbol{u}$ and $\delta\dot{\boldsymbol{u}}$ are smaller than one. So the second order item $\left(\frac{\partial^2\boldsymbol{R}}{\partial^2\boldsymbol{u}}\right)_0\delta^2\boldsymbol{u},\left(\frac{\partial^2\boldsymbol{R}}{\partial^2\dot{\boldsymbol{u}}}\right)_0\delta^2\dot{\boldsymbol{u}},\left(\frac{\partial^2\boldsymbol{R}}{\partial\boldsymbol{u}\partial\dot{\boldsymbol{u}}}\right)_0\delta\boldsymbol{u}\delta\dot{\boldsymbol{u}}$ is much less than the first order items of $\delta\boldsymbol{u}$, $\delta\dot{\boldsymbol{u}}$, and the second order items can be neglected. Finally we obtain the dynamically nonlinear POD snapshot equation:

$$\boldsymbol{A}_1\delta\dot{\boldsymbol{w}}+\boldsymbol{B}_1\delta^2\boldsymbol{w}+\boldsymbol{H}_1\delta\boldsymbol{w}+\boldsymbol{G}_1\delta\boldsymbol{u}+(\boldsymbol{C}_1+\boldsymbol{E}_1)\delta\dot{\boldsymbol{u}}=0,\tag{15}$$

where

$$\boldsymbol{A}_1=\boldsymbol{A}(\boldsymbol{u}_0,\boldsymbol{o})+\left(\frac{\partial A}{\partial\boldsymbol{u}}\right)_0\delta\boldsymbol{u}+\left(\frac{\partial A}{\partial\dot{\boldsymbol{u}}}\right)_0\delta\dot{\boldsymbol{u}},$$

$$\boldsymbol{B}_1=\frac{1}{2}\left(\frac{\partial^2\boldsymbol{R}}{\partial^2\boldsymbol{w}}\right)_0,$$

$$\boldsymbol{H}_1=\left(\frac{\partial\boldsymbol{R}}{\partial\boldsymbol{w}}\right)_0+\left(\frac{\partial A}{\partial\boldsymbol{u}}\right)_0\delta\dot{\boldsymbol{u}}+\left(\frac{\partial^2\boldsymbol{R}}{\partial\boldsymbol{w}\partial\boldsymbol{u}}\right)_0\delta\boldsymbol{u}+\left(\frac{\partial^2\boldsymbol{R}}{\partial\boldsymbol{w}\partial\dot{\boldsymbol{u}}}\right)_0\delta\dot{\boldsymbol{u}}.$$

The partial derivatives should be computed previously according to the background steady flow. The inputs are $\delta\boldsymbol{u}$, $\delta\dot{\boldsymbol{u}}$, and the outputs are $\delta\boldsymbol{w}$, which can be solved by the Newton-Raphson technique. $\delta\boldsymbol{w}$ is the nonlinear snapshot required for ROM construction.

2.2.2 *NPOD/ROM for the aeroelastic system*

Suppose snapshot matrix is $\boldsymbol{W}$, and the POD kernel matrix $\boldsymbol{R}=\boldsymbol{W}\boldsymbol{W}^{\mathrm{T}}$. Using the POD algorithm to obtain a r-dimension proper orthogonal space $\boldsymbol{\Psi}_r$, which is the fluid mode, and projecting the eq. (8) to $\boldsymbol{\Psi}_r$, we can get the nonlinear NPOD/ROM for aeroelastic system:

$$\begin{aligned}&\boldsymbol{A}_1\boldsymbol{\Psi}_r\delta\dot{\boldsymbol{w}}_r+\boldsymbol{B}_1\boldsymbol{\Psi}_r^2\delta^2\boldsymbol{w}+\boldsymbol{H}_1\boldsymbol{\Psi}_r\delta\boldsymbol{w}_r\\&\quad+\boldsymbol{G}_1\delta\boldsymbol{u}+(\boldsymbol{C}_1+\boldsymbol{E}_1)\delta\dot{\boldsymbol{u}}=0,\\&\mathrm{M}\ddot{\boldsymbol{u}}+\mathbf{C}\dot{\boldsymbol{u}}+\boldsymbol{K}_s\boldsymbol{u}-q_\infty\boldsymbol{P}\boldsymbol{\Psi}_r\delta\boldsymbol{w}_r=0,\end{aligned}\tag{16}$$

where

$$\boldsymbol{P}=\frac{\partial\boldsymbol{f}^{\mathrm{ext}}}{\partial\boldsymbol{w}}(\boldsymbol{u}_0,\boldsymbol{w}_0),K_s=K_0-\frac{\partial\boldsymbol{f}^{\mathrm{ext}}}{\partial\boldsymbol{u}}(\boldsymbol{u}_0,\boldsymbol{w}_0).$$

s is the order of the structure equation which can be reduced by structure modes. The order of the system (16) is just 2*s*+*r*, which is much smaller than the original system. It is very convenient to analyze the stability of the aeroelastic system and observe the time response from the NPOD/ ROM. It is much more simple and efficient than CFD/CSD coupled computation.

2.3 Traditional POD/ROM

Retain the first order factors of eq. (15), and the full order dynamically linearized snapshot equation can be obtained:

$$\boldsymbol{A}_0\delta\dot{\boldsymbol{w}}+\boldsymbol{H}\delta\boldsymbol{w}+\boldsymbol{G}\delta\boldsymbol{u}+\left(\boldsymbol{C}+\boldsymbol{E}\right)\delta\dot{\boldsymbol{u}}=0, \tag{17}$$

$$\begin{aligned}\boldsymbol{H}&=\frac{\partial\boldsymbol{R}}{\partial\boldsymbol{w}}\left(\boldsymbol{w}_0,\boldsymbol{u}_0,\dot{\boldsymbol{u}}_0\right),\\ \boldsymbol{G}&=\frac{\partial\boldsymbol{R}}{\partial\boldsymbol{u}}\left(\boldsymbol{w}_0,\boldsymbol{u}_0,\dot{\boldsymbol{u}}_0\right),\\ \boldsymbol{C}&=\frac{\partial\boldsymbol{R}}{\partial\dot{\boldsymbol{u}}}\left(\boldsymbol{w}_0,\boldsymbol{u}_0,\dot{\boldsymbol{u}}_0\right),\\ \boldsymbol{E}&=\boldsymbol{w}_0\frac{\partial A}{\partial\boldsymbol{u}}\left(\boldsymbol{u}_0\right).\end{aligned} \tag{18}$$

The linearization fluid eq. (17) can be transformed into the state space equation:

$$\begin{cases}\dot{\boldsymbol{w}}=\boldsymbol{A}\boldsymbol{w}+\boldsymbol{B}\left[\boldsymbol{v}\quad\boldsymbol{u}\right]^{\mathrm{T}},\\ \boldsymbol{F}=\boldsymbol{C}\boldsymbol{w}.\end{cases} \tag{19}$$

$\boldsymbol{A}=-\boldsymbol{A}_0^{-1}\boldsymbol{H}$, $\boldsymbol{B}=-\boldsymbol{A}_0^{-1}\left[\boldsymbol{E}+\boldsymbol{C}\quad\boldsymbol{G}\right]$, $\boldsymbol{C}$=$\boldsymbol{P}$. Use the algorithm in section 2 to obtain *r*-dimension proper orthogonal subspace $\boldsymbol{\Psi}_r$, project the eq. (13) into $\boldsymbol{\Psi}_r$ and then we can obtain the reduced fluid model:

$$\begin{cases}\dot{\boldsymbol{w}}_r=\boldsymbol{\Psi}_r^{\mathrm{T}}\boldsymbol{A}\boldsymbol{\Psi}_r\boldsymbol{w}_r+\boldsymbol{\Psi}_r^{T}\boldsymbol{B}\boldsymbol{y},\\ \boldsymbol{F}=\boldsymbol{P}\boldsymbol{\Psi}_r\boldsymbol{w}_r.\end{cases} \tag{20}$$

By placing eq. (20) into eq. (19), the traditional time-domain POD/ROM of aeroelastic system can be represented as follows:

$$\begin{bmatrix}\dot{\boldsymbol{w}}_r\\ \dot{\boldsymbol{v}}\\ \dot{\boldsymbol{u}}\end{bmatrix}=\begin{bmatrix}-\boldsymbol{\Psi}_r^{\mathrm{T}}\boldsymbol{A}_0^{-1}\boldsymbol{H}\boldsymbol{\Psi}_r & -\boldsymbol{\Psi}_r^{\mathrm{T}}\boldsymbol{A}_0^{-1}\left(\boldsymbol{E}+\boldsymbol{C}\right) & -\boldsymbol{\Psi}_r^{\mathrm{T}}\boldsymbol{A}_0^{-1}\boldsymbol{G}\\ \frac{1}{2}\rho_\infty V_\infty^2\bar{\boldsymbol{M}}^{-1}\boldsymbol{P}\boldsymbol{\Psi}_r & -\bar{\boldsymbol{M}}^{-1}\bar{\boldsymbol{C}} & -\bar{\boldsymbol{M}}^{-1}\bar{\boldsymbol{K}}_S\\ 0 & \boldsymbol{I} & 0\end{bmatrix}\begin{bmatrix}\boldsymbol{w}_r\\ \boldsymbol{v}\\ \boldsymbol{u}\end{bmatrix}, \tag{21}$$

as can be seen, the traditional time-domain POD/ROM is just one special case of the NPOD/ROM.

3 Numerical simulation

3.1 NLR 7301 airfoil aeroelastic model

3.1.1 NLR 7301 airfoil model

A typical two-degree-freedom pitch and plunge aerofoil section aeroelastic model is depicted in Figure 1. The pitch movement around the elastic axis is represented by the angle of attack α and the plunge movement relative to the horizontal surface is denoted by *h*. The NLR 7301 airfoil section aero-elastic model was tested intensively by Dietz et al. [9] and the model parameters are presented in their articles. Transonic aeroelastic experiments in wind tunnel were conducted for various Mach numbers and angles of attack, and LCO was observed in some special instances. The model was also numerically simulated by Thomas et al. [10] to validate their aeroelastic solver for LCO prediction at different Mach numbers and reduced velocities. So the NLR 7301 airfoil section aeroelastic model is good enough for validating the capability of the new NPOD/ROM.

3.1.2 Snapshots comparison between linearization and nonlinear equation

A general multi-block structure gird POD/ROM solver including CFD solver, CFD/CSD coupled solver and linearized snapshot solver was developed by the authors and validated by many aeroelastic models including the agard 445.6 wing model [11], which indicated the developed solvers were accurate and efficient. In order to investigate the characteristics of the different fidelity models, the unsteady lift coefficient response of NRL 7301 aeroelastic model was computed by the direct CFD solver, linearized snapshot solver and second-order nonlinear snapshot solver. The flow conditions indicate *Ma*=0.76, α=0°, *h*=0, V^*=0.375 and the aerodynamic O-type mesh is 400×100.

Figure 2 displays the lift coefficient response of different fidelity solvers at a given pitch vibration movement with very small amplitude. The responses of different models are shown to be very close. It answers why the dynamically linearized model is accurate enough to predict the unsteady aerodynamics at the small disturbance [6]. It also points out the essentials why the conventional or first order POD/

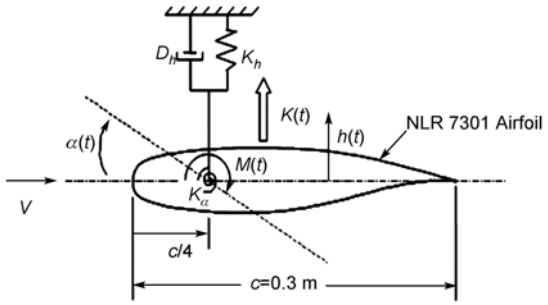

Figure 1 The typical airfoil section (pitch and plunge) aeroelastic model.

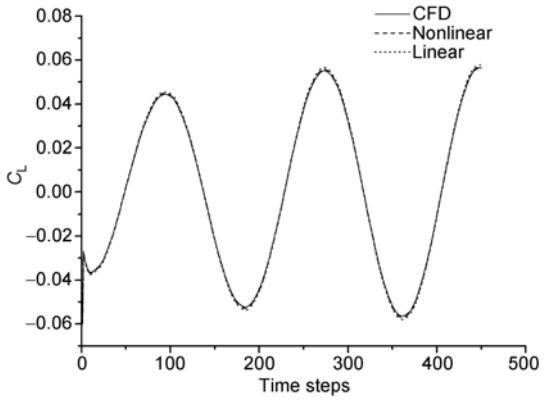

Figure 2 Lift coefficient response (small disturbance).

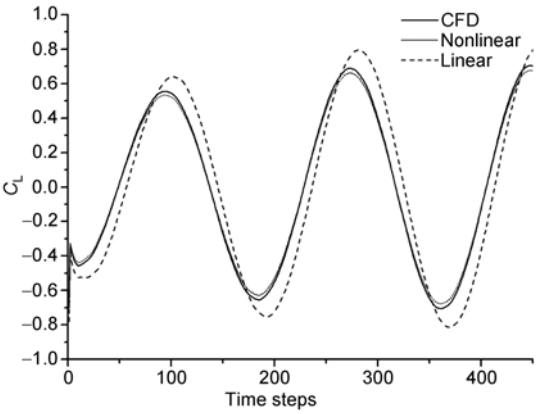

Figure 3 Lift coefficient response (large disturbance).

ROM can model the traditional aeroelastic phenomena very well such as flutter and gust response, because they are still small perturbation to the steady reference mean flow.

Next we enlarge the amplitude of pitch movement ten times which is a large disturbance to the steady mean flow field and observe the unsteady aerodynamics response again. Figure 3 shows the unsteady lift coefficient response of direct CFD, linearization and nonlinear snapshot equation. It is clearly seen that the linearized snapshot equation has obvious errors in amplitude and also some little shifts in frequency, while the nonlinear snapshot equation still shows good performance in contrast to the direct CFD solver. The simulation results indicate why the traditional time-domain POD/ROM is very sensitive to the flow parameters.

3.1.3 LCO prediction

Eqs. (15) and (17) are used to solve the snapshots with the time step of 5×10^{-5} s and 200 step response is obtained from Dirac triangle impulse function for each mode displacement and mode velocity for each structure mode movements under the condition of Ma=0.75, α=0°. The correlation coefficient matrix of the snapshots for some observed grids are computed and most of the elements are no more than 0.05, which indicated that the snapshots are not correlated. And then 80-order POD/ROM and NPOD/ROM for the aeroelastic system are constructed.

We hope to meet the LCO at the reduced velocity V^*=0.376 which is above the flutter point. In this case, the conventional time-domain linear POD/ROM failed while the NPOD/ROM catches the LCO. Figure 4 shows the pitch responses of LCO predicted by the NPOD/ROM and the direct CFD/CSD couple solver. Figure 5 is the plunge movement of the LCO. The local zoom map is also plotted. The amplitude error of the LCO predicted by the NPOD/ROM is less than 8% of those by the CFD/CSD solver. The LCO is very close to Tang's results [12] which were computed by the CFL3D solver. The consistent response shows the capability and accuracy of NPOD/ROM for LCO prediction.

Similar to the traditional POD/ROM, the computation efficiency of NPOD/ROM is also excellent. For LCO prediction of the two-dimensional viscous NLR 7301 aeroelastic model, the computation cost is reduced from the order of hours for direct CFD/CSD solver to on the order of seconds for NPOD/ROM. We also find that the NPOD/ROM can predict the response very well even at α=3.5° which is far from the steady background flow at α=0° where the ROM is constructed, while the traditional POD/ROM fails to do so. This means that the NPOD/ROM is much more robust to

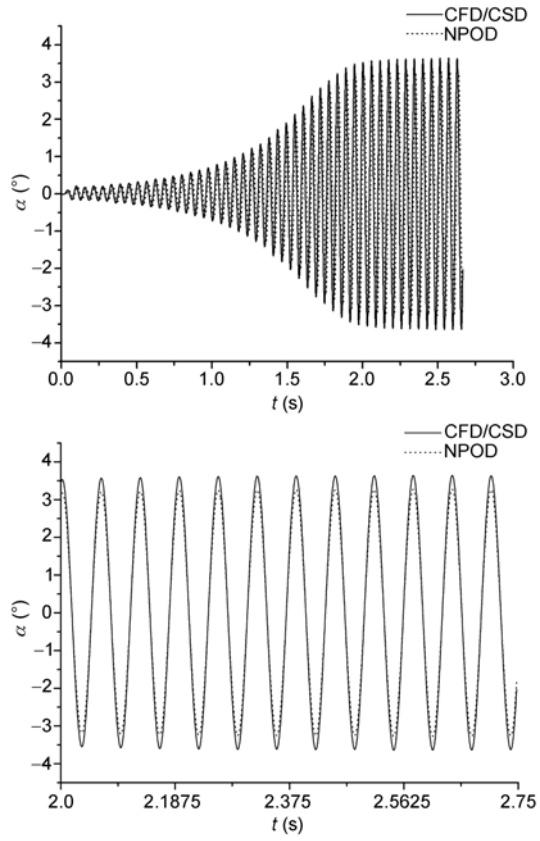

Figure 4 Pitch movement predicted by NPOD vs. CFD/CSD solver.

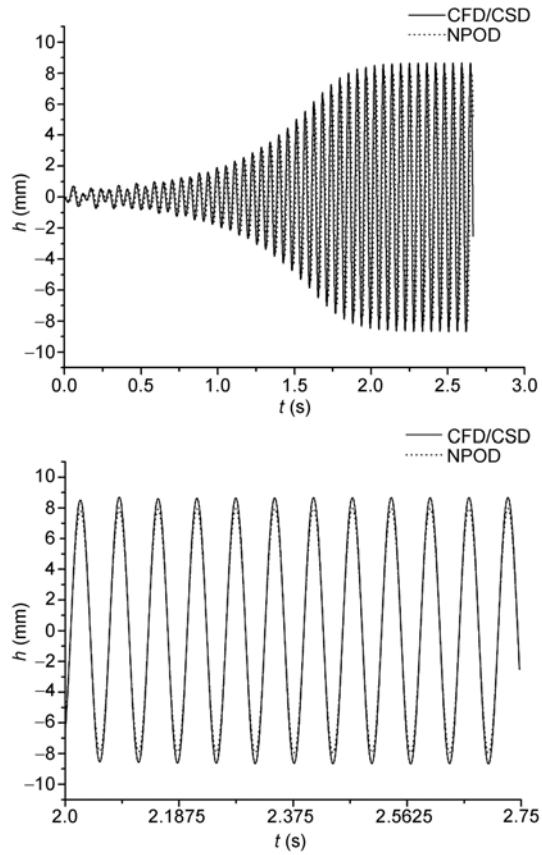

Figure 5 Plunge movement predicted by NPOD vs. CFD/CSD solver.

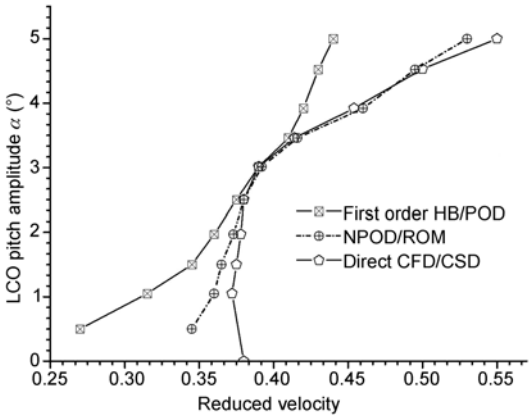

Figure 6 LCO response trend predicted by different models.

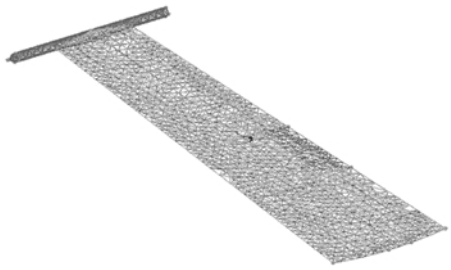

Figure 7 surface mesh of the Goland+ wing/strore system.

flow parameter variation than traditional POD/ROM. This is benifit from the second order items of the dynamically nonlinear snapshots equation.

3.1.4 LCO response trend prediction

In this section, the 100-order NPOD/ROM is constructed at Ma=0.75, α=0.2°. And then we compute the pitch amplitude of LCO trend in different reduced order velocities. Figure 6 gives the LCO pitch amplitude vs. reduced velocity predicted by different models. As can be seen, the first order HB/POD developed by Thomas et al. [13] can capture LCO very well in some instances such as the reduced velocity 0.37–0.41, but there are still obviously large errors in other conditions. The first-order ROM is unsuitable for LCO accurate trend prediction. However, the LCO trend predicted by NPOD/ROM is very close to the direct CFD/CSD solver in most instances. It indicates again that NPOD/ROM is the enhanced version of the traditional first order POD/ROM when the flow state is far away from the steady background flow where the ROM is constructed.

3.2 Goland+ wing/store aeroelastic system

3.2.1 Goland+ wing/store model

The Goland+ wing/store model is a variant of the heavy Goland wing developed as a transonic flutter test case by Eastep and Olsen [14]. The Goland+ wing is rectangular and cantilevered from an infinite midplane. The wing semi-span is 6.096 m, the chord is 1.8288 m and the thickness-to-chord ratio is 0.04. The elastic axis is located 0.6096 m from the leading edge. The airfoil section is constant over the spanwise extent of the wing and is chosen to be symmetric. There is a 3.048 m long, 0.127 m diameter cylindrical store with an elliptic nose cone centered on the wing tip. The frequencies of the first six structure modes are 1.7051, 3.0516, 9.200, 10.906, 16.271 and 22.861 Hz. The aerodynamic grid is about 200k and the surface mesh of Goland+ wing/store model is shown in Figure 7.

3.2.2 LCO prediction

The aeroelastic response of the wing Goland+ wing/store aeroelastic system was also investigated by Gregory et al. [15] through the FLUENT solver. At a Mach number 0.92 and an angle of attack zero, snapshots matrix was first computed. The elements correlation coefficient matrix of the snapshots Matrix for some observed grids are no more than 0.06, which indicates that the snapshots are not correlated. And then a 300-order NPOD/ROM was constructed. We use our coupled CFD/CSD solver and the 300-order NPOD/ROM to simulate limit cycle oscillation of Goland+ wing after the general mode velocity 0.1 is given to the second structure mode. The six structure modes are simul-

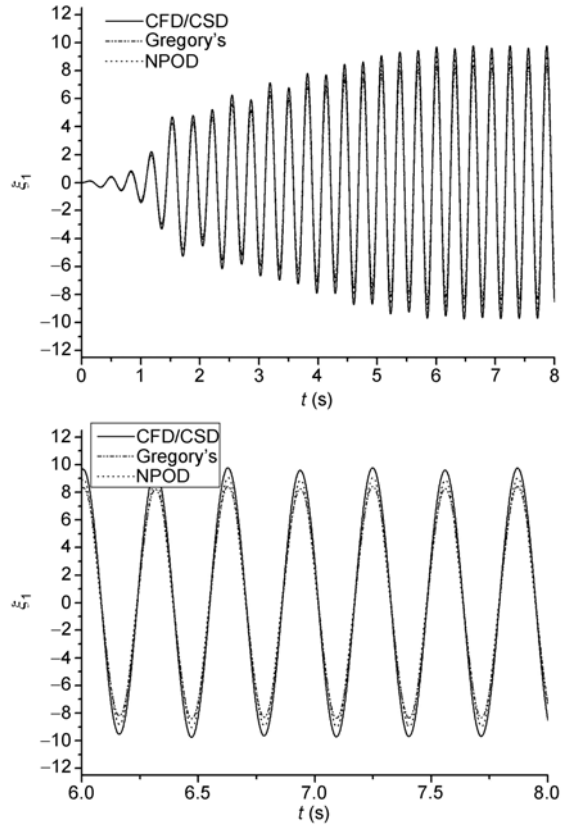

Figure 8 LCO of the first structure mode.

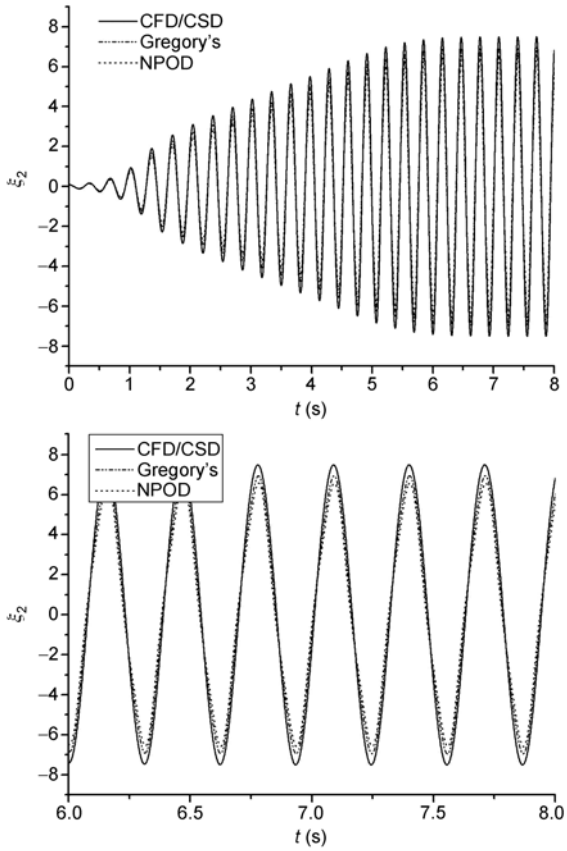

Figure 9 LCO of the first structure mode.

taneously computed, but only the general mode displacement of the first two modes are given in Figures 8 and 9.

As can be seen, our solvers can capture the LCO which is very close to Gregory's results. From the right zoom picture of Figure 8 and 9, it is found that the results of NPOD/ROM are consistent with the direct CFD/CSD solver with the errors no more than 8.1% which is accurate for limit cycle oscillation simulation. The total order for the direct CFD/CSD couple solver is 753660 which is so large, took us more than one day to obtain the LCO results. While the 300-order NPOD/ROM just takes several minutes to capture the LCO with excellent accuracy. The computation efficient NPOD/ROM is very convenient for large scale analysis such as LCO trend prediction or sensitivity analysis of nonlinear aeroelasticity.

4 Conclusion

The NPOD/ROM, a new nonlinear reduced order model in the time domain for computational fluid dynamic flow solver is investigated. The construction method of NPOD/ROM for aeroelastic system is obtained by the Taylor series expansion of the flow solver together with proper orthogonal decomposition method. The efficiency and capability for NPOD/ROM to predict the LCO is demonstrated by the NRL 7301 aeroelastic experimental model and Goland+ wing/store system. The simulation results show that the NPOD/ROM can predict the aeroelastic response very well with excellent computation efficiency, even under the condition far from the steady background flow where the ROM is constructed. The robustness will benefit flow control or near real time aeroelastic simulation such as virtual flutter flight experiment. The next step is to enhance the capability of NPOD/ROM for modeling those cases with more flow parameters varying individually or simultaneously such as Mach number, and angel of attack or bank.

This work was supported by the National Natural Science Foundation of China (Grant No. 10902082) and New Faculty Research Foundation of Xi'an Jiaotong University.

1 Lucia D J, Beran P S, Silva W A. Reduced-order modeling: New approaches for computational physics. Prog Aero Sci, 2004, 40: 51–117
2 Thomas J P, Dowell E H, Hall K C. Modeling viscous transonic limit cycle oscillation behavior using a harmonic balance approach. J Aircraft, 2004, 41: 1266–1274
3 Thomas J P, Dowell E H, Hall K C. Three-dimensional transonic aeroelasticity using proper orthogonal decomposition-based reduced order models. J Aircraft, 2003, 40: 544–551
4 Lieu T, Farhat C, Lesoinne M. Reduced-order fluid/structure modeling of a complete aircraft configuration. Comput Methods Appl Mech Eng, 2006: 5730–5742
5 Lai K L, Tsai H M. Reduced-order based flutter analysis for complex aeroelastic systems. AIAA Paper, 2008, AIAA-2008-6240
6 Dowell E H, Edwards J, Strganac T. Nonlinear aeroelasticity. J Aircraft, 2003, 40: 857–874

7 Hu G, Dowell E H. Physics-based identification, modeling and management infrastructure for aeroelastic limit-cycle oscillations. In: US Air Force Annual Structural Dynamics Conference. Arlington, CA: AIAA, 2008
8 Dowell E H, Thomas J P, Hall K C. Transonic limit cycle oscillation analysis using reduced order aerodynamic models. J Fluids Struct, 2004, 19: 17–27
9 Dietz G, Schewe G, Mai H. Experiments on heave/pitch limit-cycle oscillations of a supercritical airfoil close to the transonic dip. J Fluids Struct, 2004, 19: 1–16
10 Thomas J P, Dowell E H, Hall K C. Modeling limit cycle oscillations for an NLR 7301 airfoil aeroelastic configuration including correlation with experiment. J Aircraft, 2004, 41: 1266–1274
11 Chen G, Li Y M, Yan G R, et al. A fast aeroelastic response prediction method based on proper orthogonal decomposition reduced order model (In Chinese). J Astronuat, 2009, 30: 1765–1769
12 Tang L, Bartels R E, Chen P C, et al. Numerical investigation of transonic limit cycle oscillations of a two-dimensional supercritical wing. J Fluids Struct, 2003: 29–41
13 Thomas J P, Dowell E H, Hall K C. Using automatic differentiation to create a nonlinear reduced order model of a computational fluid dynamic solver. AIAA Paper, 2008, AIAA -2008-2322
14 Eastep F E, Olsen J J. Transonic flutter analysis of a rectangular wing with conventional airfoil sections. AIAA J, 1980, 18: 1159–1164
15 Gregory H P, Raymond C M, Beran P S. Analysis of store effects on limit-cycle oscillation. AIAA Paper, 2006, AIAA-2006-1846